International Journal of Sciences
Research Article Volume 4 - February 2015 (02)

Electrochemical Synthesis of Micrometre Amorphous Calcium Phosphate Tubes and their Transformation to Hydroxyapatite Tubes

Sridevi Brundavanam[1], Gérrard Eddy Jai Poinern[1], Derek Fawcett[1]

[1]Murdoch Applied Nanotechnology Research Group, Department of Physics, Energy Studies and Nanotechnology, School of Engineering and Energy, Murdoch University, Murdoch, Western Australia 6150, Australia Fax: +61 8 9360-6183

Abstract: Amorphous calcium phosphate tube-like structures were formed on magnesium substrates using a straightforward electrochemical process. The effect of voltage, time and the resulting hydrogen gas evolution were found to be responsible for sculpturing the tube-like structures covering the entire substrate surface. Scanning electron microscopy and Energy Dispersive Spectroscopy was used to quantify the size, shape, structure and composition of the tube-like structures. Microscopy analysis was used to develop a model to describe the mechanism behind the formation of the tube-like structures. Also investigated was a hydrothermal technique used to convert the amorphous calcium phosphate structures into hydroxyapatite. Both X-ray diffraction spectroscopy and Fourier Transform Infrared spectroscopy were used to confirm the effectiveness of the conversion process.

Keywords: Electrochemical synthesis, amorphous calcium phosphate, microstructures

1. Introduction

Amorphous calcium phosphate (ACP) is the first mineral phase that precipitates from highly saturated aqueous solutions containing calcium and phosphate ions due to its lower surface energy compared to other calcium phosphates such as octacalcium phosphate (OCP) and hydroxyapatite (HAP) [1]. Unlike other calcium phosphates, ACP is metastable, has a non-crystalline character with short-range order and lacks long-range periodic uniformity normally associated with crystalline structures [2]. Analysis of X-ray diffraction measurements have revealed that ACP has only two very broad and diffuse peaks, with a maximum occurring at a 2θ angle of 25°. No other features, normally associated with crystalline materials are observed [3]. This pattern is typical for non-crystalline or amorphous materials and confirms the lack of long-range periodic regularity of ACP. The spherical structural unit of synthetic ACP is composed of randomly assembled clusters of ions approximately 9.5Å in diameter and with the chemical composition of Ca_9 $(PO_4)_6$ [4]. Also contained within the interstices of a typical ACP particle is tightly bound water that can be as much as 20% by weight of the particle [5]. In aqueous solutions ACP particles will readily agglomerate, but are thermodynamically unstable. Therefore, ACP can be considered a transient or metastable phase that will easily transform to more thermodynamically stable crystalline calcium phosphate phases such as HAP via a process of dissolution, nucleation, and crystal growth [6]. The amorphous structure of ACP being unstable is also highly reactive and rapidly hydrolyses into more stable calcium phosphate phases in body fluids. It is due to the metastable properties of ACP that makes it more osteoconductive than hydroxyapatite and also gives it superior biodegradability when compared to tricalcium phosphate when used *in vivo* [7- 9]. The existence of ACP in aqueous solutions is governed by a number of factors such as ionic strength, pH value, temperature and the presence of contaminants or additives [10]. Stabilising metastable ACP in aqueous solutions can be achieved by the introduction of additive ions or molecules to prevent transformation to more stable crystalline calcium phosphate phases. And under *in vivo* conditions, the presence of protein based molecules and similar substances can delay the transformation of ACP due to the effects of kinetic stabilization [11]. The role of calcium binding proteins and ionic species involved in the exact mechanism of biological mineralization and transformation of ACP to HAP *in vivo* are not fully understood [12-14]. However, because of its

Published at: http://www.ijsciences.com/pub/issue/2015-02/
Article Number: v420150206; Online ISSN: 2305-3925; Print ISSN: 2410-4477

Gérrard Eddy Jai Poinern (Correspondence)
g.poinern@murdoch.edu.au
+61 8 9360-2892

biological compatibility and physiochemical properties ACP will continue to be used in the rapidly developing field of tissue engineering, dentistry and orthopaedics.

This study examines the formation ACP micrometre scale tubular structures formed on magnesium substrates during a straightforward electrochemical synthesis process. The electrodes consist of a platinum wire mesh (anode) and an Mg substrate (cathode) immersed in an electrolyte consisting of calcium nitrate and potassium di-hydrogen phosphate. Advanced characterisation techniques such as X-ray diffraction (XRD) spectroscopy, Transmission electron microscopy (TEM), Fourier Transform Infrared spectroscopy (FT-IR).

Scanning electron microscopy (SEM) and Energy Dispersive Spectroscopy (EDS) were used to determine size, morphology, composition and architecture of the formed ACP structures. Furthermore, a proposed formation model is presented to explain the growth of the ACP micrometre scale structures.

2. Materials and methods

2.1. Materials

All chemicals used in this work were supplied by Chem-Supply (Australia) and all aqueous solutions were made using Milli-Q® water (18.3 MΩ cm^{-1}) produced by an ultrapure water system (Barnstead Ultrapure Water System D11931; Thermo Scientific, Dubuque, IA).

2.2. Mg substrate surface pre-treatment

Magnesium with a purity of 99.9% was used throughout this study. The sheet was cut into rectangular strips that were 40 mm in length, 3 mm in width and 0.15 mm in thickness. The strips were polishing using 1200 grit silicon carbide (SiC) paper to remove all surface oxides and contaminants. After polishing, the strips were cleaned in 5 wt% nitric acid (HNO_3) solution followed by ultrasonically rinsing in acetone for 10 min. The acetone was then lightly rinsed from the substrates using Milli-Q® water before being allowed to air dry. After drying the weight of each substrate was recorded using an Ohaus PA214C microbalance.

2.3. Electrochemical formation of ACP surface features

The formation of ACP surface features on Mg substrates was accomplished using an electrochemical cell consisting of two electrodes and an electrolyte. The electrolyte consisted of an aqueous solution containing 0.32 M of Ca $(NO_3)_2.4H_2O$ and 0.19 M of KH_2PO_4. The electrodes used in this experimental setup consisted of a platinum wire mesh (anode) and an Mg substrate that was used as the cathode. A standard laboratory DC power supply [GW INSTEK GPS-2303] was used to supply the required voltage range with a maximum current density of 60 mA/cm^2 in the dynamic mode setting. Studies were carried out over a voltage range between 2 and 7 volts and over periods ranging from 30 s to 5 min at a room temperature of 25 ± 1 ºC. Two voltage/time procedures were followed: 1) fixed voltage (6 V) and variable time (30 s to 5 min) and, 2) fixed time 3 min and variable voltage (2 to 7 V). Both procedures were found to give sufficient experiment data for analysis purposes. After each experimental run the substrates were removed from the electrolyte, rinsed using Milli-Q® water and then air-dried before being stored ready for advanced characterisation.

2.4. Conversion of ACP structures to hydroxyapatite

Conversion of the ACP structures and coatings to hydroxyapatite (HAP) was achieved by immersing the ACP coated substrates into a 1M solution of sodium hydroxide (NaOH) at 80 ºC for 2 h. At the end of this period the substrates were removed from the electrolyte solution, washed in Milli-Q® water, and then allowed to slowly dry in air for at least 24 h. Finally, coated Mg substrates were heat treated in an electric furnace at 250 ºC for 1hour and then allowed to cool to room temperature in air. The HAP coatings were then examined using the advanced characterisation techniques discussed below.

2.5. Advanced characterisation techniques

2.5.1. X-ray diffraction (XRD) spectroscopy

XRD spectroscopy was used to study and to identify the crystalline phases present in the surface structures and coating formed during electrochemical synthesis. Spectroscopy data was recorded at room temperature, using a GBC® eMMA X-ray Powder Diffractometer [Cu K_α = 1.5406 Å radiation source] operating at 35 kV and 28 mA. The diffraction patterns were collected over a 2θ range of 20° to 60° with an incremental step size of 0.02° using flat plane geometry with 2 second acquisition time for each scan.

2.5.2. Transmission electron microscopy (TEM)

The size and morphology of ACP and HAP particles synthesized were investigated using TEM. Sample preparation consisted removing a portion of the synthesized material from the surface of the magnesium substrate. The material was then placed into small tubes containing Milli-Q® water. The tubes were then sealed and placed into an ultrasonic bath for 10 minutes. The suspensions were then filtered 2 times, and then a single drop from each sample was deposited onto its respective carbon-coated copper TEM grid using a micropipette and then allowed to slowly dry over a 24-hour period. After sample preparation a bright field TEM study was carried out

using a Phillips CM-100 electron microscope (Phillips Corporation Eindhoven, The Netherlands) operating at 80kV.

2.5.3. Fourier Transform Infrared spectroscopy (FT-IR)

FT-IR spectroscopy investigations of the synthesized ACP and HAP were carried out using a Perkin–Elmer Frontier FT-IR spectrometer with Universal Single bounce Diamond ATR attachment. Spectra were recorded in the range from 525 to 4000cm^{-1} in steps of 4 cm^{-1}.

2.5.4. Scanning electron microscopy (SEM) and Energy Dispersive Spectroscopy (EDS)

SEM was used to study the size and morphological features formed on the substrates during the creation of the surface coating. All micrographs were taken using a JCM-6000, NeoScope™ with attached energy dispersive X-ray spectroscopy. Samples were mounted on individual substrate holders using carbon adhesive tape before being sputter coated with a 2 nm layer of gold to prevent charge build up using a Cressington 208HR High Resolution Sputter coater.

3. Results and Discussions

3.1. XRD spectroscopy identification of calcium phosphate phases

XRD spectroscopy was used to identify the calcium phosphate phases formed on Mg substrates during the electrochemical synthesis process. Selections of typical XRD patterns are presented in Figure 1 (a). In Figure 1 (a) a representative XRD pattern for an Mg substrate prior to the electrochemical surface treatment is presented. Inspection of the pattern reveals three dominant peaks [(002), (101) and (102)] and two minor peaks [(100) and (110)] associated with crystalline Mg and one small peak (101) associated with $Mg(OH)_2$. Apart from $Mg(OH)_2$ no other surface contaminants were found on the substrate surfaces. During electrochemical treatment a calcium phosphate layer formed over the surface of the substrates. Subsequent XRD investigation revealed a characteristic pattern of an amorphous material as seen in Figure 1 (a). Also present in the XRD pattern are three peaks [(002), (101) and (102)] that were identified as Mg from the underlining substrate and Mg present in the ACP structures. No other calcium phosphate crystalline phases were detected in the structured surface coatings. Subsequent conversion of structured ACP surface coatings to HAP was also confirmed by XRD analysis. HAP was confirmed by the presence and identification of spectra peaks with Miller indices (002), (211) and (202) that were consistent with phases incorporated in the ICDD (International Centre for Diffraction Data) databases. Also present is the HAP pattern was the presence of (002) related peak indicating that Mg had been detected. The strong signal suggests that not only was Mg present in the substrate coating, but the underlining Mg substrate was also detected. The extensive and large crack formations in both the coating and substrate surface are believed to be responsible for the release of Mg ions and their subsequent incorporation into the forming surface structures. The incorporation of Mg ions into the coatings was also found in the EDS spectra as seen in Figure 5.

3.2. Microscopy analysis of ACP and ACP based structural features found in coatings

TEM microscopy was used to examine the structure of the initial ACP coatings found on the substrates. XRD analysis identified the formation before conversion as ACP and TEM images confirm the spherical structural nature normally associated with ACP particles as seen in Figures 2 (a) and (b). While the SEM micrograph presented in Figure 2 (c) shows the highly agglomerated nature of the ACP particles. The particles range in size from 60 nm to 250 nm, with a mean particle size of 120 nm. And because ACP is thermodynamically unstable, it tends to transform into more thermodynamically stable crystalline calcium phosphate phases and this can be seen in Figures 2 (a) and (b) with the presence of partially formed plate-like features. The partially formed plate-like features, which are indicated by blue arrows, were not detected in the XRD patterns of the initial ACP coatings. Partially formed plate-like structures were also seen in SEM images of the tubular formations as seen in Figure 2 (d), but again were not seen in the XRD spectra.

3.3. Formation of ACP structures

The electrochemical formation of ACP surface features on Mg substrates was investigated using two voltage/time procedures. The first used a fixed time period (3 min) with a variable voltage range and the second used a variable time period (30 s to 5 min) with a fixed voltage of 6 V. The first procedure investigated the effect of voltage in forming ACP surface features. The results of this study revealed that there was a voltage dependence effect and it was responsible in initiating tubular structure formations above 4 V. Below 4 V, only small numbers of hydrogen bubbles were produced and almost no calcium phosphate materials could be seen forming except for the occasional small outcrops as seen in Figures 3 (a) and (b). At this stage the surface of the Mg substrate was relative smooth and didn't show any signs of surface cracking or significant corrosion. However, from 4 V onwards, gas evolution was clearly visible across the entire surface of the substrate. With the dissolution of the Mg substrate deposits of spherical, granular shaped ACP particles and small tubules could be seen close to small cracks that had formed in the surface of the substrate as seen in Figure 3 (c). The surface cracks seen in the

substrate are the result of hydroxyl ions accumulating at the solid/liquid interface [15]. The accumulation of hydroxyl ions causes a localized region of high pH that subsequently produces the precipitation of ACP at the substrate surface. As the voltage was increased, precipitation of ACP increased and two dominant features could be seen forming. The first was surface cracking of the coating that could be seen extending down to the underling Mg substrate. And the second feature was widespread tube formation across the surface of the substrate as revealed in Figures 3 (d) to (f). An interesting feature of the tubes was the variation in diameters that ranged from 30 µm up to a maximum of around 100 µm.

During the second voltage/time procedure the voltage was maintained at 6 V while the time period ranged from 30 s to 5 min. After 30 s in the electrochemical cell, tubes could be seen forming over the entire substrate surface as seen in Figure 4 (a). In addition to the tubular features was the presence of numerous ACP plate-like particles. The plate-like features had mean diameters of around 5 µm and a thickness of around 1.5 µm and were covering the surface between the tubules as seen in Figure 4 (b). Also present was surface cracks, which were seen earlier in the variable voltage procedure for voltages above 4 V. One minute into the electrochemical procedure saw a significant increase in hydrogen evolution and an increase in size and number of tubules being formed as seen Figure 4 (c). Three minutes into the procedure saw a dramatic increase in the size and depth of cracks in the surface coating, which exposed more of the underling Mg substrate to the electrolyte, Figure (d). Also noticeable during this period was the reduced rate in new tubules being formed as indicated graphically in Figure 4 (f). At this point in time it is believed that most of the gas being formed was exiting the coating via the extensive network of large cracks covering the surface.

Figure 5 presents a SEM micrograph of a representative tubular structure formed after 3 minutes under constant voltage. EDS analysis was carried out on two locations along the length of the tube. Location (a) was taken at a position three quarters the length of the tube from the coating surface and location (b) was taken a quarter of the length from the coating surface. The spectra resulting from EDS analysis of both locations is presented in Figure 5. Both spectra are characteristic of ACP, but of particular interest is the presence of Mg in the tubular structure. The presence of Mg in the coating structures confirms the results of the XRD, which indicated the presence of Mg. Also present in both spectra was the presence of oxygen, which suggests that the presence of Mg in the coating structures could be in the form of $Mg(OH)_2$. The presence of $Mg(OH)_2$ in tubular structures could explain the existence of plate-like features seen in Figure 2 (d).

3.4. Tube Formation Model

Because of the tube-like structures present in the formation of the deposition layer, it is suspected that the release of hydrogen bubbles at the substrate surface (cathode) is one of the key factors responsible for sculpturing the deposition layer. This assumption is based on the circular geometry and consistent wall structure of the tube-like structures that appear to have been built up around an initial gas bubble residing on the metal/electrolyte interface. During the electrochemical process, the Mg substrate acting as cathode, reduces hydrogen and increases local pH. With the increase in pH, the stability of HPO_4^{2-} significantly increases compared to that of $H_2PO_4^{1-}$ and as a result the concentration of HPO_4^{2-} increases until maximum solubility is reached. Simultaneously, migration and coalescence of hydrogen at the surface of the cathode results in the formation of gaseous macroscopic bubbles as graphically presented in Figure 6 (a). It is believed that if the bubbles are small enough they will not be displaced by buoyancy. At this point, ACP begins to coat the substrate surface not occupied by bubbles and as a result the coating acts as an insulator that prevents electron flow from the substrate. However, the cathodic substrate continues to supply a current via the bubble/ACP interface that maintains hydrogen reduction, ion migration and diffusion. ACP continues being precipitated from solution and deposited around surface bubbles. At the same time hydrogen gas continues to migrate into the forming tube structure feeding the resident bubble. However, when the bubble gains sufficient volume, buoyancy forces dislodge the bubble from the substrate surface. If there is sufficient hydrogen migration a second entrapped bubble forms and so one until a steady stream of small gas bubbles leave the tube formation site. As the bubble forming process continues, the length of the tube steadily increases with the self-assembly of the ACP particles forming the tube wall structure. If electrochemical conditions are suitable and sustained then ACP deposition and growth of tube-like structures continue. However, when gas migrates into the tube bases ceases there is a rapid in flow of electrolyte resulting in rapid deposition of ACP within the tube-like structures.

3.5. Conversion of ACP coatings to HAP coatings

ACP coating structures were converted to hydroxyapatite (HAP) using a process that involved immersing substrates into sodium hydroxide at 80 ºC for 2 h followed by a 1 h thermal treatment in a furnace at 250 ºC. XRD analysis mentioned above confirmed that HAP was produced by the conversion process. Further confirmation of the effectiveness of the conversion process came from analysis of the FT-

IR spectroscopy data as presented in Figure 1 (b). Conversion of ACP to HAP was confirmed by the appearance of the peak located at 602.9 cm^{-1}, which is characteristic of PO_4^{3-} functional groups normally associated with HAP and not seen in ACP. In addition, SEM analysis of the converted coatings revealed that the tube-like structures had been transformed into urchin-like structures as seen in Figures 7 (a) and (b). TEM images of particles making up the coatings prior to conversion were spherical and ranged in size from 30 µm to 100 µm in diameter. After conversion the urchin-like structures were predominantly composed of needle-like and plate-like HAP particles. The particle width ranged from 30 nm to 90 nm, width varied between 80 nm and 200 nm and the length ranged from 450 nm up to 800 nm. Also present were a small number of granular particles ranged in size from 30 nm to 100 nm. Figure 7 (c) presents an SEM image of HAP particles found deposited over the surface of the substrate and Figure 7 (d) presents a representative TEM image of HAP particles forming in the urchin-like structures.

4. Conclusion

A straightforward electrochemical technique was used to synthesize ACP coatings with micrometre scale tube-like structures on Mg substrates. The size, structure and composition of the tube-like structures were investigated and the subsequent results were used to propose a formation model. The model explained the formation mechanism and the importance of hydrogen evolution in creating tube-like structures. Also investigated was a hydrothermal process for transforming the ACP coatings into HAP. Both XRD and FT-IR confirmed the conversion of ACP into HAP, with the ACP tube-like structures being transformed into urchin-like features. Furthermore, the spherical geometry characteristic of ACP particles was the prevailing morphology of the particles prior to the conversion process. After conversion two HAP particle morphologies were present. The first consisted of a small number of granular particles and the second consisted of plate-like particles. The nanometre scale particles composed the micrometre scale urchin-like features that dominated the substrate surface. However, further studies are needed to fully investigate the physical and chemical properties of coatings and structures formed in this preliminary study.

Acknowledgements

The authors would like to thank Mr Ken Seymour for his assistance with the XRD measurements and Mrs Sridevi Brundavanam would like to acknowledge Murdoch University for providing a PhD Scholarship to undertake her PhD studies.

Disclosure

The authors report no conflict of interest in this work.

References

1. Dorozhkin SV. Nano-dimensional and nano-crystalline apatite's and other calcium orthophosphates in biological engineering, biology and medicine. Materials, 2009; 2: 1975-2045 http://dx.doi.org/10.3390/ma2041975
2. Zhao J, Liu Y, Sun WB and Zhang H, Amorphous calcium phosphate and its application in dentistry, Chemistry Central Journal, 2011; 5(40): 1-7 http://dx.doi.org/10.1186/1752-153x-5-40
3. Boskey AL, Amorphous Calcium Phosphate: The Contention of Bone, J. Dental. Research, 1997; 76 (8): 1433-1436 http://dx.doi.org/10.1177/00220345970760080501
4. Betts F, Blumenthal NC, Posner AS, Becker GL, Lehninger AL: Atomic structure of intracellular amorphous calcium phosphate deposits. Proc. Natl. Acad. Sci. 1975; 72: 2088-2090 http://dx.doi.org/10.1073/pnas.72.6.2088
5. Termine JD, Eanes ED: Comparative chemistry of amorphous and apatetic calcium phosphate preparations. Calcif. Tissue Res. 1972; 10: 171-197 http://dx.doi.org/10.1007/bf02012548
6. Eanes ED, Termine JD, and Nylen MU. An electron microscopic study of the formation of amorphous calcium phosphate and its transformation to crystalline apatite. Calcif. Tissue Res. 1973; 12:143-158 http://dx.doi.org/10.1007/bf02013730
7. Li YB, Li DX, Weng WJ. Amorphous calcium phosphate and its biomedical application. J. Inorgan. Mater, 2007; 22: 775-782
8. Poinern GEJ, Brundavanam R, Le X, Nicholls PK, Cake MA, Fawcett D. The synthesis, characterisation and in vivo study of a bioceramic for potential tissue regeneration applications. Scientific Reports, 2014; 4, 6235: 1-9 http://dx.doi.org/10.1038/srep06235
9. Dorozhkin SV. Calcium Orthophosphates as Bioceramics: State of the Art. J. Funct. Biomater. 2010; 1: 22-107 http://dx.doi.org/10.3390/jfb1010022
10. Zhao J, Liu Y, Sun WB and Yang X. First detection, characterization, and application of amorphous calcium phosphate in dentistry. Journal of Dental Sciences, 2012; 7: 316-323 http://dx.doi.org/10.1016/j.jds.2012.09.001
11. Boskey AL, Posner AS. Magnesium stabilization of amorphous calcium phosphate: a kinetic study. Mater. Res. Bull. 1974; 9: 907-916 http://dx.doi.org/10.1016/0025-5408(74)90169-x
12. Beniash E, Metzler RA, Lam RS, Gilbert PU. Transient amorphous calcium phosphate in forming enamel. J Struct Biol 2009; 166: 133-143 http://dx.doi.org/10.1016/j.jsb.2009.04.002
13. Wilt FH. Developmental biology meets material science: Morphogenesis of biomineralized structures. Development Biology, 2005; 280: 15-25 http://dx.doi.org/10.1016/j.ydbio.2005.01.019
14. Wang L, Nancollas GH. Dynamics of biomineralization and biodemineralization. Met. Ions. Life. Sci. 2010; 4: 413-456 http://dx.doi.org/10.1002/9780470986325.ch13
15. Gray-Munro JE & Strong M. The mechanism of deposition of calcium phosphate coatings from solution onto magnesium alloy AZ31. Journal of Biomedical Materials Research Part A, 2008; DOI: 10.1002/jbm.a.32107 12 pages http://dx.doi.org/10.1002/jbm.a.32107

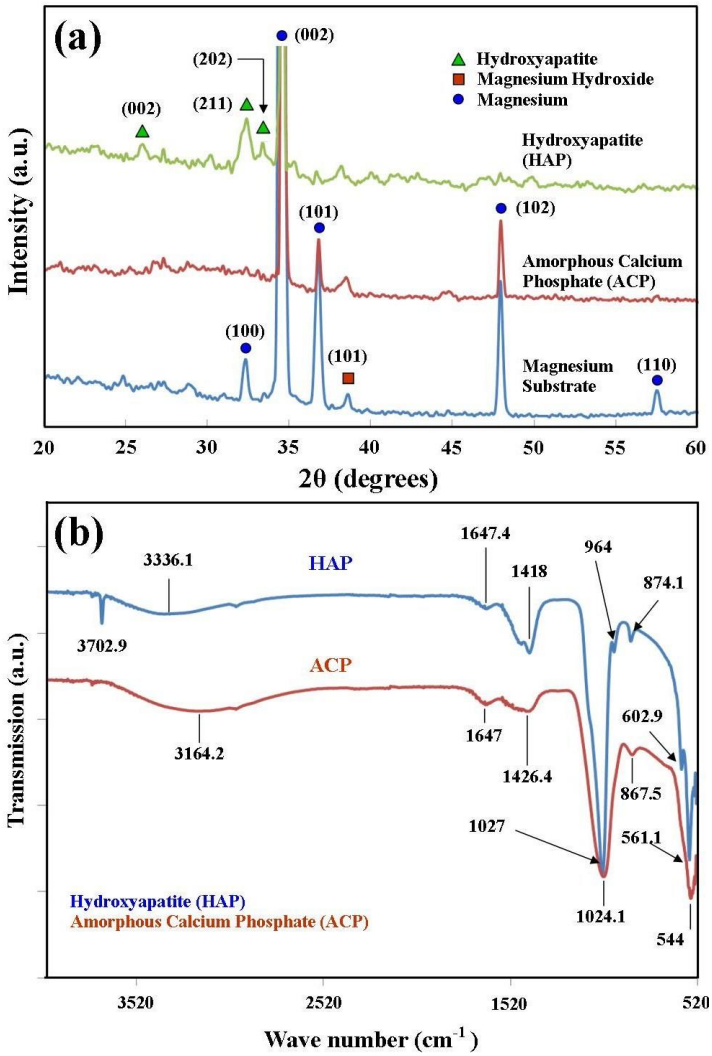

Figure 1 (a) Representative XRD patterns of Mg substrates, ACP and HAP coatings and (b) Results of a comparative FT-IR study confirming the conversion of ACP to HAP

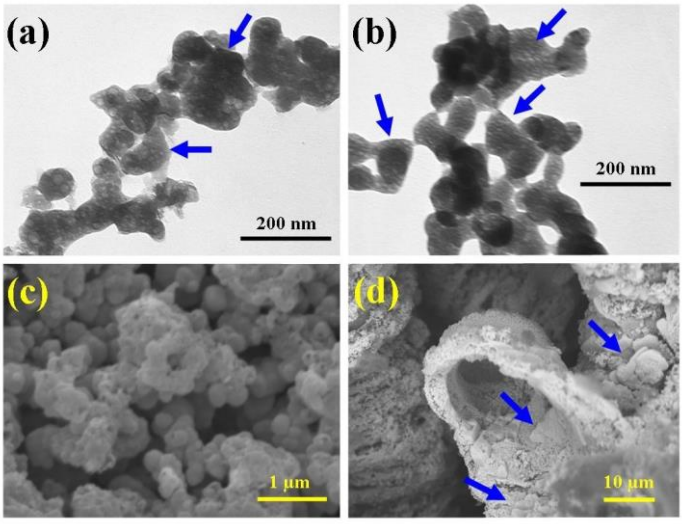

Figure 2 (a) and (b) TEM images of ACP particles, (c) SEM image of agglomerated ACP particles and (d) ACP tubular structure composed of ACP particles and partially formed plate-like particles.

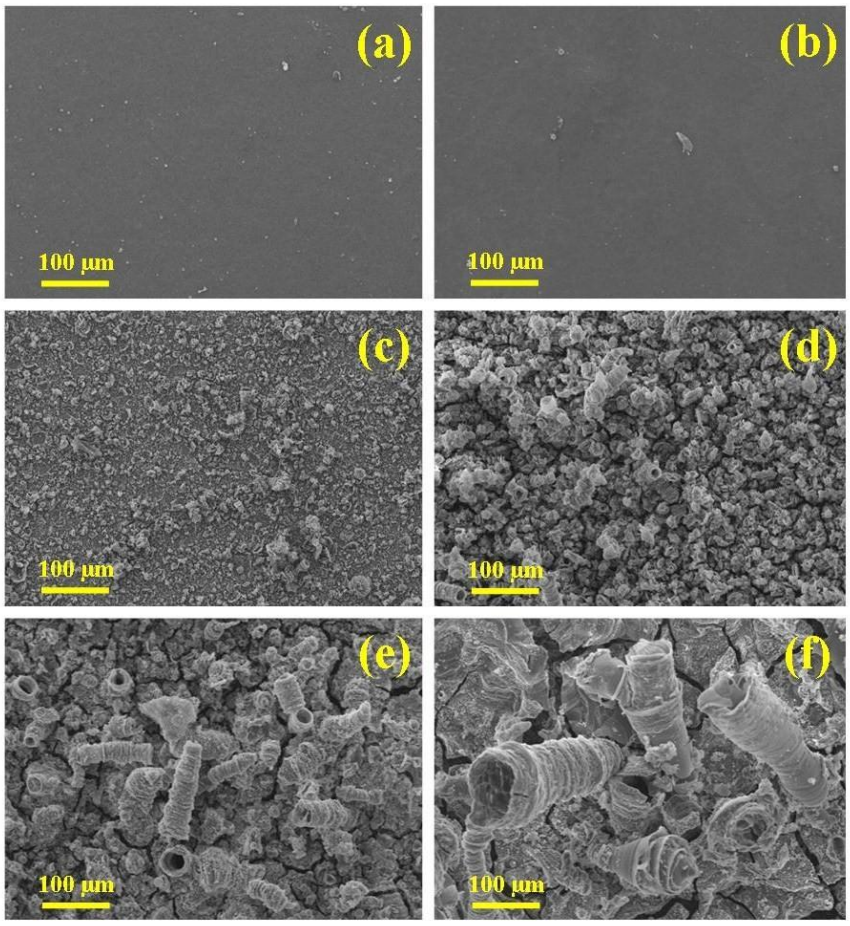

Figure 3 Growth of ACP tubules over a period of 3 min at voltages of (a) 2, (b) 3, (c) 4, (d) 5, (e) 6 and (f) 7 volts.

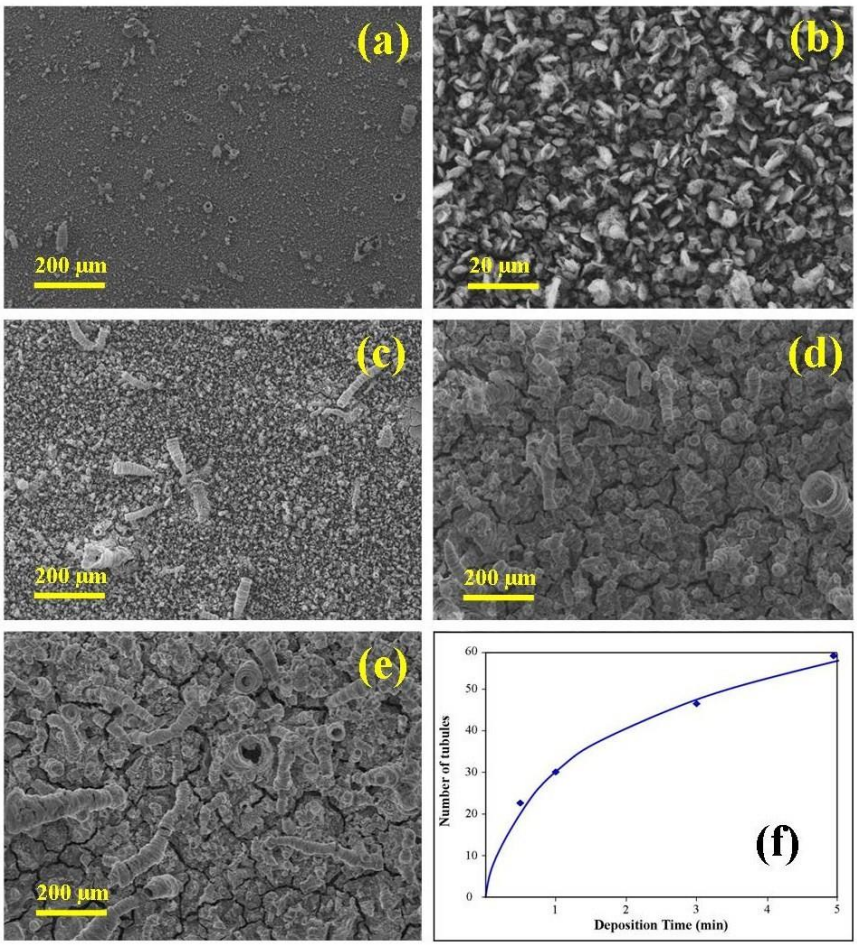

Figure 4 SEM micrographs recording the growth of ACP tubules using the constant voltage procedure (6Volts): (a) and (b) 30 s; (c) 1 min; (d) 3 min; (e) 5 min, and (f) number of tubular structures formed as a function of deposition time.

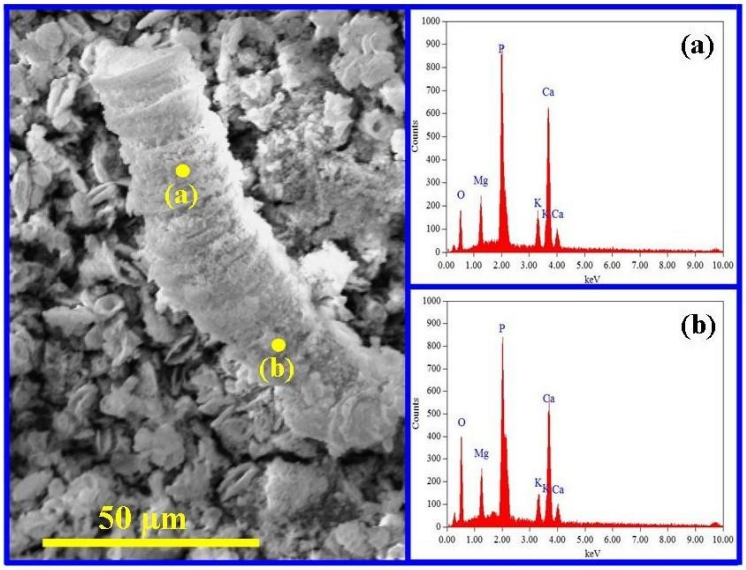

Figure 5 EDS analysis showing the chemical composition of two separated locations along the length of a typical tube-like structure formed during the electrochemical process.

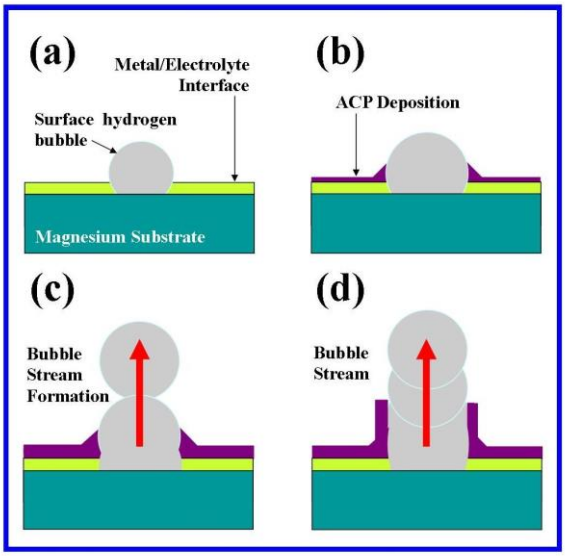

Figure 6 Tubule formation mechanism: (a) a typical gas bubble residing on the metal/electrolyte interface, (b) build up of deposited ACP around the bubble, (c) bubble stream formation and (d) wall structure formation.

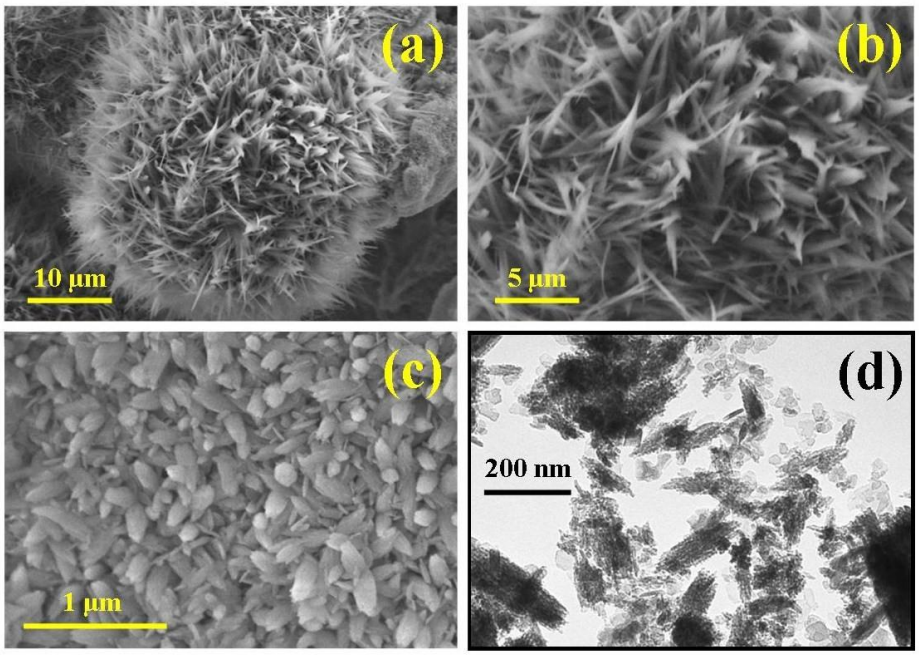

Figure 7 (a) a representative ACP tube-like structure after HAP conversion; (b) enlarged view of urchin-like formation after conversion; (c) enlarged SEM image of substrate surface showing HAP particles, and (d) TEM image of HAP particles formed after conversion.